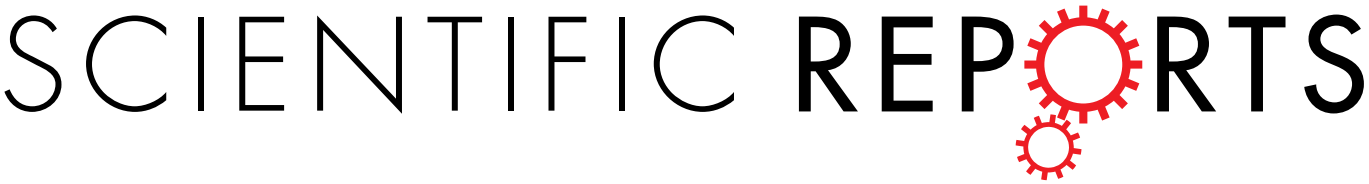

OPEN

Impact of isovalent and aliovalent substitution on the mechanical and thermal properties of $Gd_2Zr_2O_7$

Received: 14 March 2017
Accepted: 15 June 2017
Published online: 25 July 2017

S. Zhang[1], H. B. Zhang[2], F. A. Zhao[3], M. Jiang[1], H. Y. Xiao[1], Z. J. Liu[4] & X. T. Zu[3]

In this study, a density functional theory method is employed to investigate the effects of isovalent and aliovalent substitution of Sm^{3+} on the phase stability, thermo-physical properties and electronic structure of $Gd_2Zr_2O_7$. It is shown that the isovalent substitution of Sm^{3+} for Gd^{3+} results in the formation of $Gd_2Zr_2O_7$-$Sm_2Zr_2O_7$ solid solution, which retains the pyrochlore structure and has slight effects on the elastic moduli, ductility, Debye temperature and band gap of $Gd_2Zr_2O_7$. As for the aliovalent substitution of Sm^{3+} for Zr^{4+} site, a pyrochlore-to-defect fluorite structural transition is induced, and the mechanical, thermal properties and electronic structures are influenced significantly. As compared with the $Gd_2Zr_2O_7$, the resulted $Gd_2Sm_yZr_{2-y}O_7$ compositions have much smaller elastic moduli, better ductility and smaller Debye temperature. Especially, an amount of electrons distribute on the fermi level and they are expected to have larger thermal conductivity than $Gd_2Zr_2O_7$. This study suggests an alternative way to engineer the thermo-physical properties of $Gd_2Zr_2O_7$ and will be beneficial for its applications under stress and high temperature.

The rare-earth zirconates, with chemical formula $A_2Zr_2O_7$ (A = Y or another rare earth elements)[1,2], exhibit ordered pyrochlore-type structure or defect fluorite-type structure, which is mainly governed by the ionic radii of A^{3+} and Zr^{4+}[3]. They have attracted the attention of many researchers, due to their good chemical and mechanical stability, excellent catalytic activity, high ionic conductivity, ferromagnetism, luminescence as well as strong resistance to amorphization under irradiation[4–8]. Owing to these outstanding properties, the rare-earth zirconates have a wide range of technical applications, e.g., ceramic thermal barrier coating[9,10], oxidation catalyst[5,11], solid electrolyte[12], hosts of actinides in nuclear waste[13] and oxygen gas sensor[14].

Of the zirconate pyrochlores, $Gd_2Zr_2O_7$ is of special interest due to its good thermo-physical properties[15–19]. Shimamura *et al.* have measured the thermal expansion of a series of zirconate pyrochlores employing high-temperature X-ray diffraction and found that the thermal expansion coefficient of $Gd_2Zr_2O_7$ is larger than other zirconates during the temperature range of 400–1600 °C[20]. The thermal conductivity of rare-earth zirconates has been investigated by Wang *et al.*[21], who reported that the thermal conductivity of 1.15–1.43 W/mK for $Gd_2Zr_2O_7$ is lower than that of $Yb_2Zr_2O_7$, $Dy_2Zr_2O_7$ and 7YSZ between 25 °C and 800 °C. In recent years, a great number of investigations have been carried out on substitution of lanthanides for Gd-site to engineer the thermo-physical properties of $Gd_2Zr_2O_7$[22–25]. Guo *et al.* synthesized $(Gd_{1-x}Yb_x)_2Zr_2O_7$ (x = 0, 0.1, 0.3, 0.5, 0.7) using solid state reaction and suggested that the thermal conductivity of 0.88–1.00 W/mk for $(Gd_{1-x}Yb_x)_2Zr_2O_7$ is about 20% lower than that of $Gd_2Zr_2O_7$ (1.18 W/mk) at 1400 °C[26]. Wan *et al.* predicted that, among the $(La_xGd_{1-x})_2Zr_2O_7$ ($0 \le x \le 1$) systems, the $LaGdZr_2O_7$ has the minimum thermal conductivity, which is about 20–25% lower than that of $Gd_2Zr_2O_7$[18]. In recent years, both Liu *et al.*[19]. and Pan *et al.*[23] reported that the thermal diffusivity of $(Sm_xGd_{1-x})_2Zr_2O_7$ ($0 \le x \le 1$) are lower than those of pure $Gd_2Zr_2O_7$ and $Sm_2Zr_2O_7$. Especially, $Sm_2Zr_2O_7$-$Gd_2Zr_2O_7$ solid solutions have lower Young's modulus than $(La_xGd_{1-x})_2Zr_2O_7$ ($0 < x < 1$) at room temperature and larger thermal expansion coefficients than $(Gd_{1-x}Yb_x)_2Zr_2O_7$ (x = 0, 0.1, 0.3, 0.5, 0.7) from 300 °C to 900 °C[18,19,23,26]. These investigations are mainly experimental studies, and the related theoretical investigations are relatively much fewer[27,28].

[1]School of Physical Electronics, University of Electronic Science and Technology of China, Chengdu, 610054, China. [2]Institute of Nuclear Physics and Chemistry, Chinese Academy of Engineering Physics, Mianyang, 621900, China. [3]Institute of Fundamental and Frontier Sciences, University of Electronic and Technology of China, Chengdu, 610054, China. [4]Department of Physics, Physics, Lanzhou City University, Lanzhou, 730070, China. Correspondence and requests for materials should be addressed to H.Y.X. (email: hyxiao@uestc.edu.cn) or Z.J.L. (email: lzjcaep@126.com)

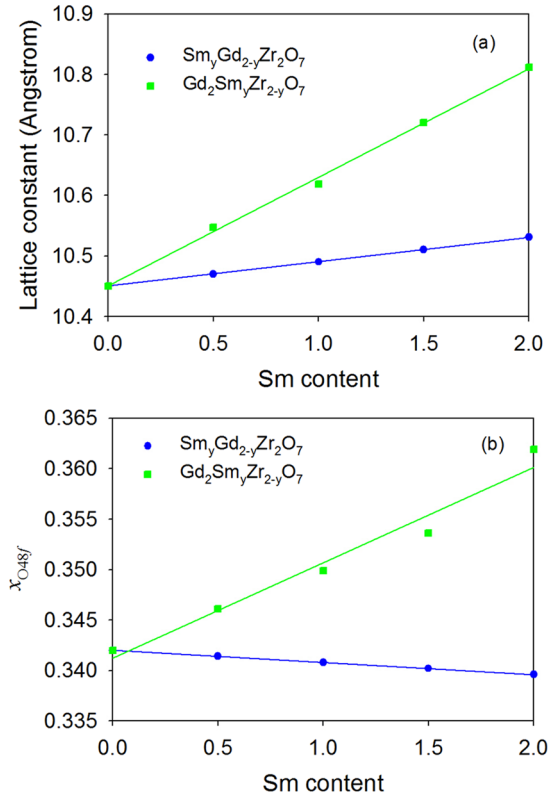

Figure 1. Variation of (**a**) lattice constants and (**b**) positional parameter x_{O48f} for $Sm_yGd_{2-y}Zr_2O_7$ and $Gd_2Sm_yZr_{2-y}O_7$ ($0 \leq y \leq 2$) as a function of Sm content.

Compounds	d < Gd-O_{48f}>	d < Gd-O_{8b}>	d < Sm-O_{48f}>	d < Sm-O_{8b}>	d < Zr-O_{48f}>
$Gd_2Zr_2O_7$	2.478	2.263	—	—	2.083
$Sm_{0.5}Gd_{1.5}Zr_2O_7$	2.482	2.257	2.497	2.297	2.084
$SmGdZr_2O_7$	2.485	2.252	2.503	2.289	2.085
$Sm_{1.5}Gd_{0.5}Zr_2O_7$	2.495	2.245	2.506	2.286	2.086
$Sm_2Zr_2O_7$	—	—	2.514	2.280	2.087
$Gd_2Sm_{0.5}Zr_{1.5}O_7$	2.482	2.280	2.253	—	2.087
Gd_2SmZrO_7	2.387	2.309	2.329	—	2.124
$Gd_2Sm_{1.5}Zr_{0.5}O_7$	2.394	2.327	2.299	—	2.096
$Gd_2Sm_2O_7$	2.426	2.341	2.262	—	—

Table 1. The bonding distances (Å) between atoms in $Sm_yGd_{2-y}Zr_2O_7$ and $Gd_2Sm_yZr_{2-y}O_7$ ($0 \leq y \leq 2$).

Very recently, the Th^{4+} ion incorporation into Gd^{3+} and Zr^{4+} sites in $Gd_2Zr_2O_7$ was investigated by first-principles calculations[28]. Unexpectedly, the aliovalent substitution of Th^{4+} for Gd^{3+} turns out to be thermodynamically stable and such substitution even results in better thermo-physical properties than the pure $Gd_2Zr_2O_7$[28]. This thus arouses our interest that whether the aliovalent substitution of Ln^{3+} (Ln = lanthanide elements) for Zr^{4+} sites are energetically and mechanically stable or not? If yes, will the substitution of Ln^{3+} for Zr^{4+} sites cause different thermo-mechanical properties from the isovalent substitution of Ln^{3+} for Gd^{3+} sites? In this study, we choose Sm^{3+} as a model and investigate the phase stability and thermo-physical properties of $Gd_2Zr_2O_7$ with isovalent and aliovalent substitution of Ln^{3+} for Gd^{3+} and Zr^{4+} sites by employing the density functional theory (DFT) method. It reveals that the $Sm_yGd_{2-y}Zr_2O_7$ retains the pyrochlore structure and the isovalent substitution of Sm^{3+} for Gd^{3+} sites influences slightly the mechanical and thermal properties of $Gd_2Zr_2O_7$. On the other hand, the aliovalent substitution of Sm^{3+} for Zr^{4+} sites induces pyrochlore-to-fluorite structural transition and affects significantly the elastic moduli, Debye temperature and thermal conductivity. The presented results provide a new way to tune the thermo-physical properties of $Gd_2Zr_2O_7$ and will have important implications in advancing the further related experimental and theoretical studies for its applications under high temperature.

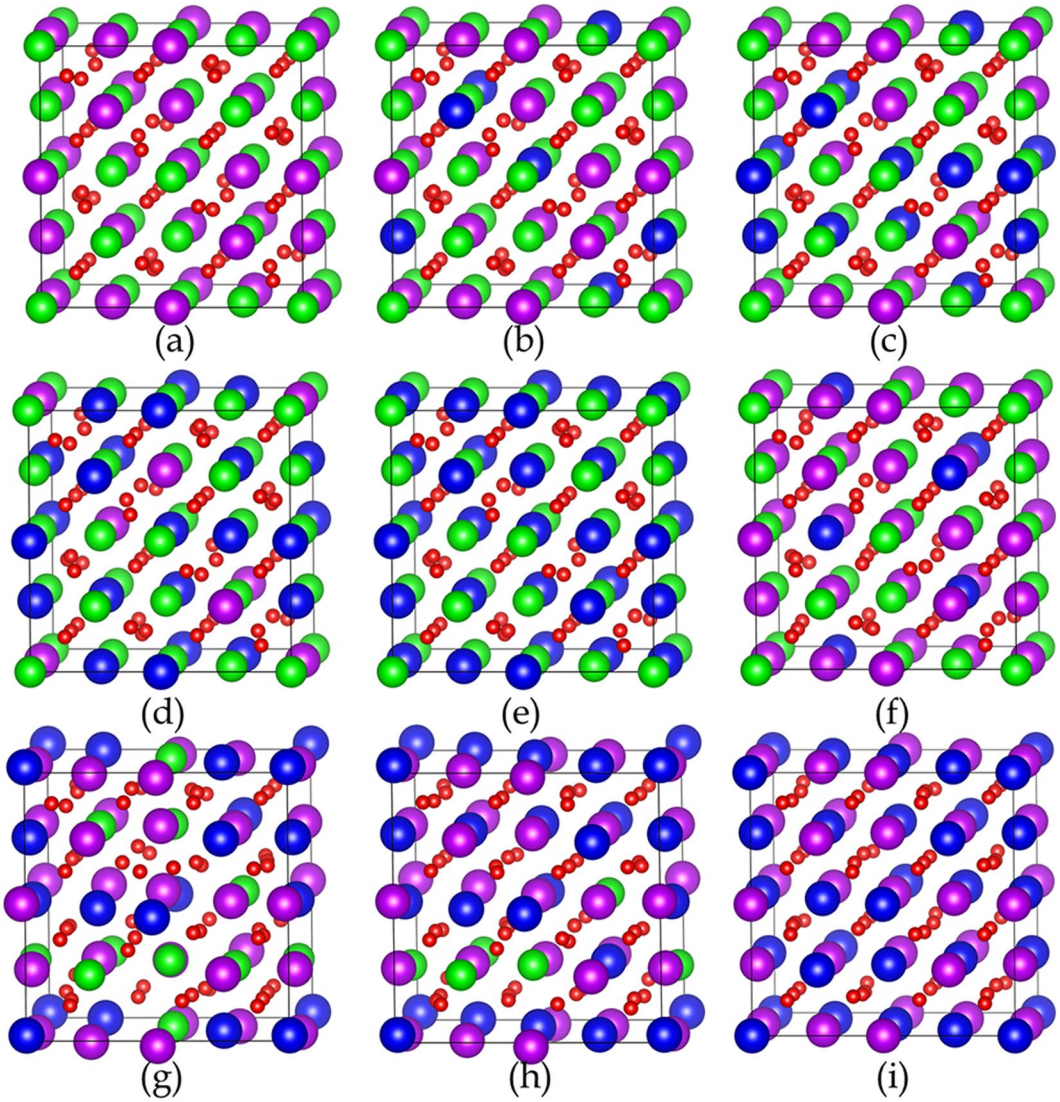

Figure 2. Schematic view of the optimized configurations for (**a**) $Gd_2Zr_2O_7$, (**b**) $Sm_{0.5}Gd_{1.5}Zr_2O_7$, (**c**) $SmGdZr_2O_7$, (**d**) $Sm_{1.5}Gd_{0.5}Zr_2O_7$, (**e**) $Sm_2Zr_2O_7$, (**f**) $Gd_2Sm_{0.5}Zr_{1.5}O_7$, (**g**) Gd_2SmZrO_7, (**h**) $Gd_2Sm_{1.5}Zr_{0.5}O_7$, (**i**) $Gd_2Sm_2O_7$. The blue, purple, green and red spheres represent Sm, Gd, Zr and O atoms, respectively.

Results and Discussion

Structural stability of $Sm_yGd_{2-y}Zr_2O_7$ and $Gd_2Sm_yZr_{2-y}O_7$ ($0 \leq y \leq 2$). In this study, Sm substitution for both Gd-site and Zr-site in $Gd_2Zr_2O_7$ with different concentrations are considered, resulting in $Sm_yGd_{2-y}Zr_2O_7$ and $Gd_2Sm_yZr_{2-y}O_7$ (y = 0, 0.5, 1, 1.5, 2). The geometrical structures of $Sm_yGd_{2-y}Zr_2O_7$ and $Gd_2Sm_yZr_{2-y}O_7$ are optimized firstly. In order to test whether local density approximation (LDA)[29] or generalized gradient approximation (GGA)[30] is more appropriate to describe the exchange-correlation interaction between electrons, both LDA and GGA methods are employed to relax the structures of $Gd_2Zr_2O_7$ and $Sm_2Zr_2O_7$. For $Gd_2Zr_2O_7$, the lattice constant a_0 and x_{O48f} obtained by LDA are 10.451 Å and 0.342, respectively, agreeing well with the experimental values of $a_0 = 10.472$ Å and $x_{O48f} = 0.345$[31,32]. As compared with the LDA results, the values of $a_0 = 10.641$ Å and $x_{O48f} = 0.339$ calculated by GGA deviate much more from the experimental results. As for $Sm_2Zr_2O_7$, the LDA calculations yield a lattice constant of 10.531 Å and an x_{O48f} parameter of 0.34, which are also comparable with the experimental data of $a_0 = 10.514$ Å and $x_{O48f} = 0.342$[31,32]. On the other hand, the GGA results of $a_0 = 10.715$ Å and $x_{O48f} = 0.337$ are in bad agreement with the experimental measurement. Obviously, the structural parameters obtained by LDA are in better agreement with experiments than the GGA method. The LDA method, thus, is employed in all the subsequent calculations. The calculated lattice constant a_0 and x_{O48f} for $Sm_yGd_{2-y}Zr_2O_7$ and $Gd_2Sm_yZr_{2-y}O_7$ as a function of Sm content are plotted in Fig. 1a and b, respectively. As Sm substitutes for Gd-site in $Gd_2Zr_2O_7$, it is found that the resulted $Sm_yGd_{2-y}Zr_2O_7$ compositions remain the ideal pyrochlore structure. Especially, the lattice constant a_0 and the O_{48f} positional parameter x_{O48f} increase and decrease linearly with the increasing Sm concentration, suggesting that he lattice parameters of $Sm_yGd_{2-y}Zr_2O_7$ follow well the Vegard's law, i.e., $a(Sm_yGd_{2-y}Zr_2O_7) = \frac{2-y}{2} \times a(Gd_2Zr_2O_7) + \frac{y}{2} \times a(Sm_2Zr_2O_7)$. These results indicate that the $Gd_2Zr_2O_7$-$Sm_2Zr_2O_7$ solid solution is formed by Sm substitution into Gd-site in $Gd_2Zr_2O_7$,

Compounds		C_{11}	C_{12}	C_{44}	B	G	E
$Gd_2Zr_2O_7$	LDA	325.6	126.3	94.0	192.7	96.2	247.5
	LDA + U	316.9	123.0	94.7	187.6	95.6	245.2
	LDA + SOC	325.6	126.6	93.7	192.9	96.0	247.0
	Exp.[23]						234
	Exp.[57]						241
	Exp.[20]				174	92	236
	Other cal.[36]	289	103	85	165	88	224
$Sm_{0.5}Gd_{1.5}Zr_2O_7$	LDA	320	125	95	190	96	247
$SmGdZr_2O_7$	LDA	318	125	95	189	95	245
$Sm_{1.5}Gd_{0.5}Zr_2O_7$	LDA	316	125	95	188	95	244
$Sm_2Zr_2O_7$	LDA	314.2	126.2	96.2	188.8	95.3	244.7
	LDA + U	276.9	114.2	112.6	168.4	98.8	248.0
	LDA + SOC	315.3	127.4	95.9	190.0	95.1	244.5
	Exp.[23]						231
	Exp.[20]				173	91	231
	Other cal.[36]	286	107	88	169	89	226
$Gd_2Sm_{0.5}Zr_{1.5}O_7$	LDA	253	130	82	171	73	192
Gd_2SmZrO_7	LDA	209	140	68	163	52	141
$Gd_2Sm_{1.5}Zr_{0.5}O_7$	LDA	190	139	59	156	42	116
$Gd_2Sm_2O_7$	LDA	165	144	61	151	31	87

Table 2. Elastic constants (C_{11}, C_{12}, C_{44}, in GPa), bulk modulus (B, in GPa), shear modulus (G, in GPa) and Young's modulus (E, in GPa) of $Sm_yGd_{2-y}Zr_2O_7$ and $Gd_2Sm_yZr_{2-y}O_7$ ($0 \leq y \leq 2$).

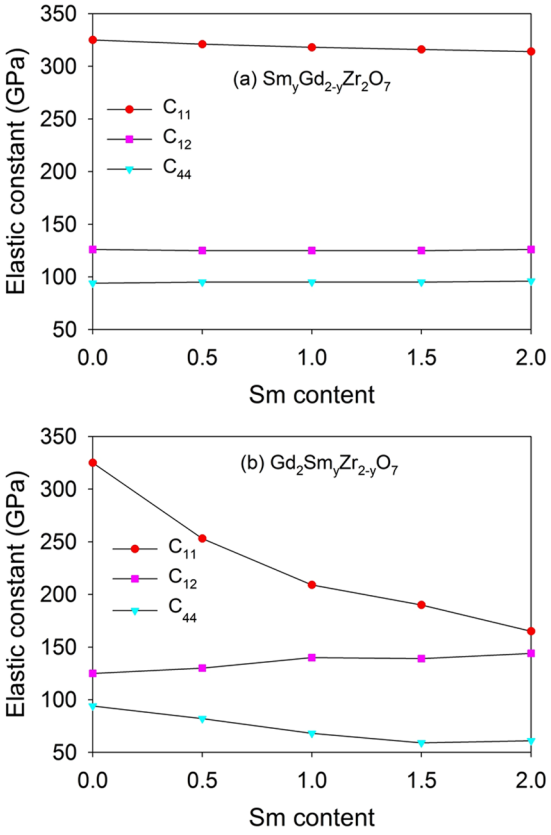

Figure 3. Variation of elastic constants (C_{11}, C_{12} and C_{44}) for (**a**) $Sm_yGd_{2-y}Zr_2O_7$ and (**b**) $Gd_2Sm_yZr_{2-y}O_7$ ($0 \leq y \leq 2$) with Sm content.

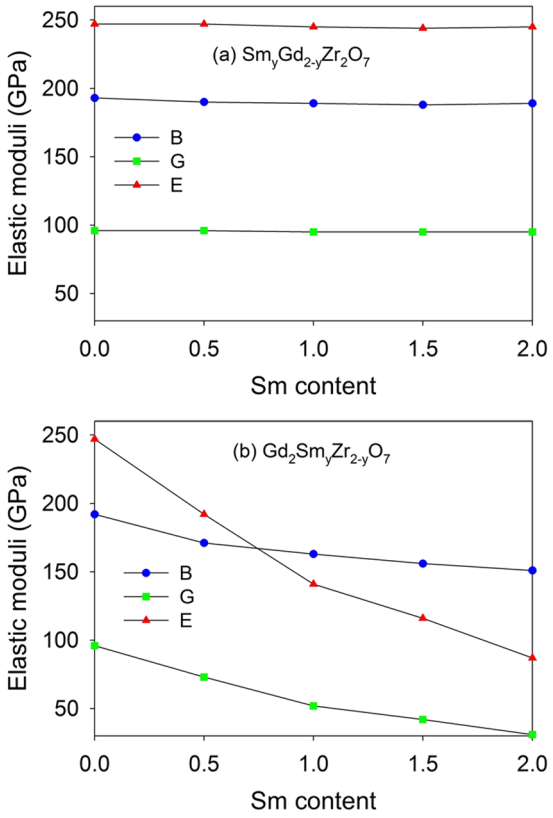

Figure 4. Variation of elastic moduli for (**a**) $Sm_yGd_{2-y}Zr_2O_7$ and (**b**) $Gd_2Sm_yZr_{2-y}O_7$ ($0 \leq y \leq 2$) as a function of Sm content. B: bulk modulus; G: shear modulus; E: Young's modulus.

Compounds		G/B	A^U	v_m	Θ	σ
$Gd_2Zr_2O_7$	Our Cal.	0.499	0.00420	4833.5	612.9	0.286
	Exp.[48]					0.276
	Exp.[20]				513.3	0.274
	Other cal.[36]					0.273
$Sm_{0.5}Gd_{1.5}Zr_2O_7$		0.505	0.00085	4855.2	614.4	0.284
$SmGdZr_2O_7$		0.504	0.00042	4864.9	614.5	0.284
$Sm_{1.5}Gd_{0.5}Zr_2O_7$		0.504	0.00009	4880.8	615.3	0.284
$Sm_2Zr_2O_7$	Our Cal.	0.505	0.00063	4918.3	618.8	0.284
	Exp.[48]					0.277
	Exp.[20]				513.3	0.278
	Other cal.[36]					0.274
$Gd_2Sm_{0.5}Zr_{1.5}O_7$	Our Cal.	0.428	0.097	4220.6	530.5	0.313
Gd_2SmZrO_7	Our Cal.	0.320	0.566	3583.7	447.4	0.356
$Gd_2Sm_{1.5}Zr_{0.5}O_7$	Our Cal.	0.270	0.920	3230.2	399.5	0.376
$Gd_2Sm_2O_7$	Our Cal.	0.205	4.738	2786.4	341.7	0.404

Table 3. Pugh's indicator (G/B), elastic anisotropy index (A^U), sound wave velocity (v_m, in m/s), Debye temperature (Θ, in K) and Poisson's ratio (σ) of $Sm_yGd_{2-y}Zr_2O_7$ and $Gd_2Sm_yZr_{2-y}O_7$ ($0 \leq y \leq 2$).

agreeing well with the experimental observation[19]. Experimentally, Liu *et al.* also found that the lattice constants increase linearly with different compositions for $(Sm_xGd_{1-x})_2Zr_2O_7$ system from $x = 0$ ($Gd_2Zr_2O_7$) to $x = 1.0$ ($Sm_2Zr_2O_7$), and the $Gd_2Zr_2O_7$ and $Sm_2Zr_2O_7$ ceramics are infinitely solid solution[19]. As Sm substitutes for Zr-site, i.e. $Gd_2Sm_yZr_{2-y}O_7$, the lattice constants increase more significantly than the case of $Sm_yGd_{2-y}Zr_2O_7$ and there is a small deviation from the Vegard's law. It is noticeable that the x_{O48f} of $Gd_2Sm_yZr_{2-y}O_7$ increases remarkably with the increasing Sm content instead of decreasing as the case of $Sm_yGd_{2-y}Zr_2O_7$. In $A_2B_2O_7$ pyrochlores, the x_{O48f} positional parameter can be used to describe the degree of distortion of < B-O > octahedron and it is located within the range of 0.3125 to 0.375. Generally, the material with x_{O48f} closer to 0.3125 has the ordered pyrochlore

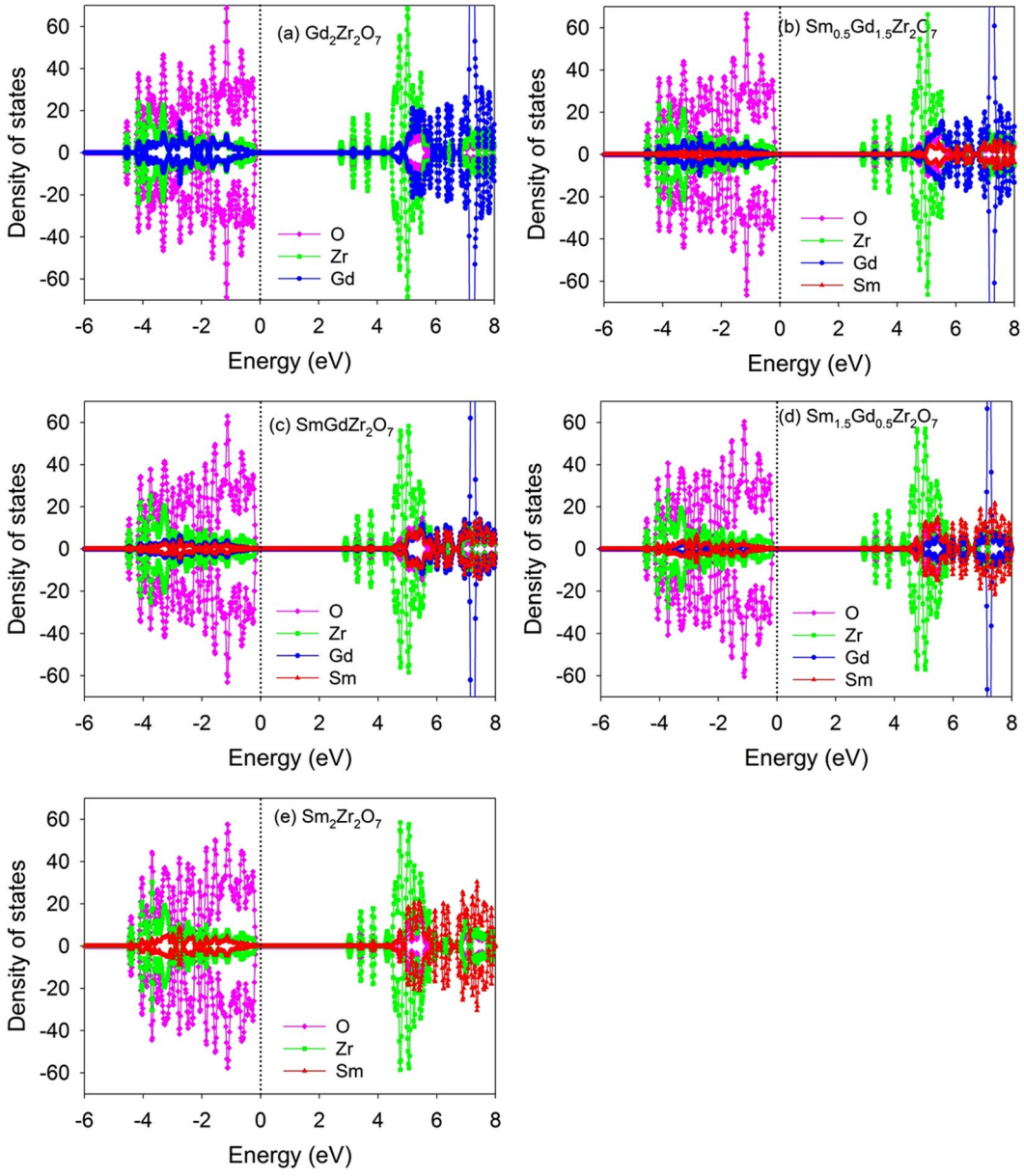

Figure 5. Projected density of state distribution for $Sm_yGd_{2-y}Zr_2O_7$ (y = 0, 0.5, 1, 1.5, 2). The Fermi level is located at 0 eV.

structure and the one with x_{O48f} closer to 0.375 is more likely to undergo a transition from pyrochlore to defect-fluorite structure[31,33–35]. Our calculations show that the x_{O48f} for $Gd_2Sm_yZr_{2-y}O_7$ with high content of Sm approaches to be 0.375, implying that order-disorder transition may occur in the systems. The schematic view of optimized configurations of $Sm_yGd_{2-y}Zr_2O_7$ and $Gd_2Sm_yZr_{2-y}O_7$ is illustrated in Fig. 2. As can be seen in the figure, $Sm_yGd_{2-y}Zr_2O_7$ still maintains the pyrochlore-type structure, while $Gd_2Sm_yZr_{2-y}O_7$ exhibits defective fluorite-type structure due to the significant disordering of the anions. These results suggest that Sm substitution for Gd-site has minor effects on the pyrochlore structure of $Gd_2Zr_2O_7$, as evidenced by the small changes in the < Gd-O > and < Zr-O > bonding distances shown in Table 1. On the other hand, structural transformation from ordered pyrochlore to disordered defect-fluorite structure is induced by the substitution of Sm for Zr-site, which is accompanied by the weakened interaction of $< Sm\text{-}O_{48f} >$ and $< Gd\text{-}O_{8b} >$ bonds (see Table 1).

In the literature, it has been reported that the Madelung binding energy reduces with the increasing x_{O48f} and the thermal expansion increases with the decreasing Madelung binding energy[20]. Considering that $Gd_2Sm_yZr_{2-y}O_7$ has larger x_{O48f} than $Sm_yGd_{2-y}Zr_2O_7$, we thus suggest that smaller Madelung binding energy exists in the $Gd_2Sm_yZr_{2-y}O_7$ and they probably have larger thermal expansion coefficient. Meanwhile, the disordering of oxygen ions in $Gd_2Sm_yZr_{2-y}O_7$ may increase the phonon scattering, which will reduce the mean free path of the phonon and result in small phonon thermal conductivity.

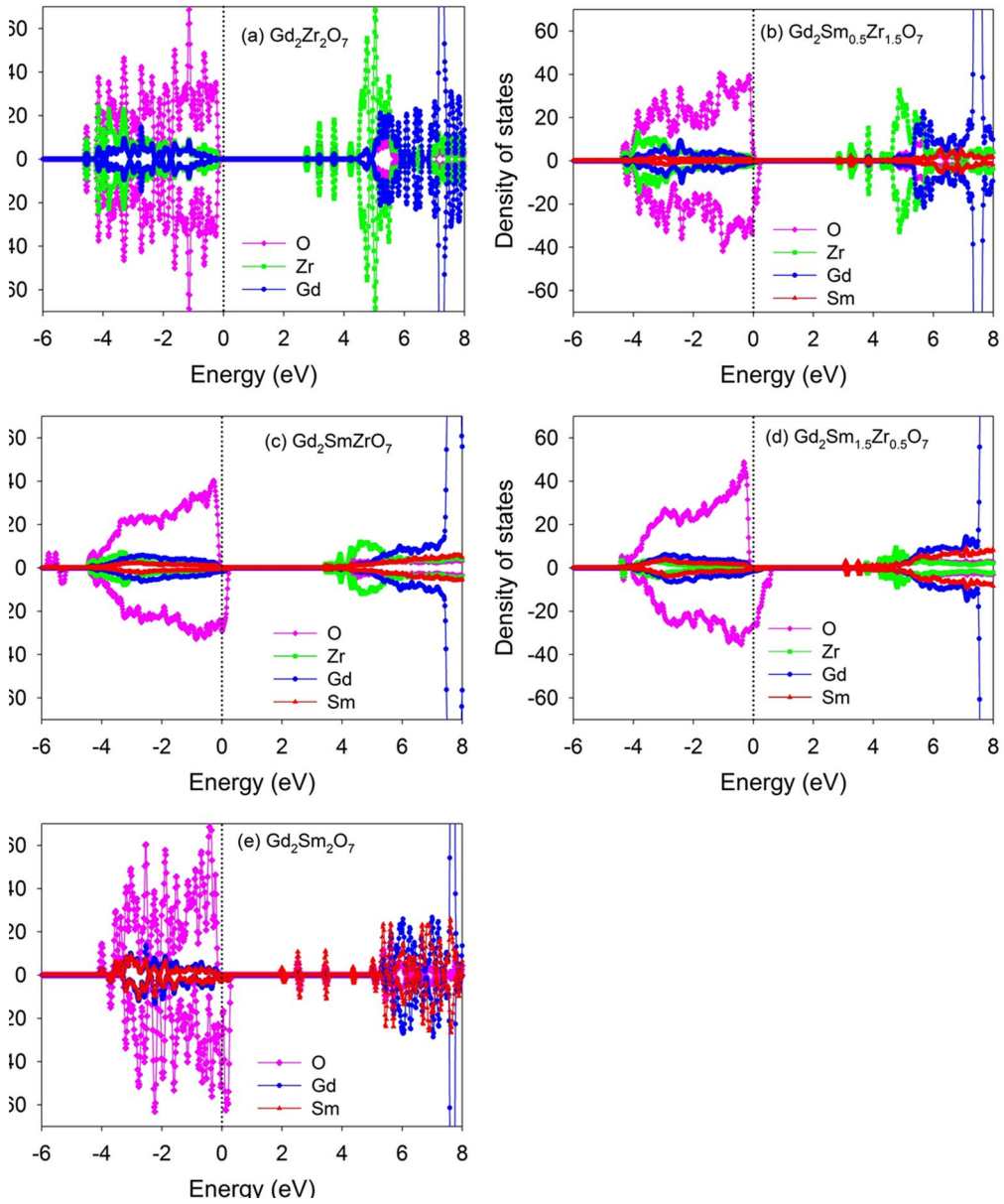

Figure 6. Projected density of state distribution for $Gd_2Sm_yZr_{2-y}O_7$ (y = 0, 0.5, 1, 1.5, 2). The Fermi level is located at 0 eV.

Elastic constants and elastic moduli of $Sm_yGd_{2-y}Zr_2O_7$ and $Gd_2Sm_yZr_{2-y}O_7$ ($0 \leq y \leq 2$). In order to investigate the mechanical properties of $Sm_yGd_{2-y}Zr_2O_7$ and $Gd_2Sm_yZr_{2-y}O_7$ compounds, we further calculate their elastic constants based on the optimized structures. For a cubic crystal, there are three independent elastic constants, i.e. C_{11}, C_{12} and C_{44}, where C_{11} refers to the uniaxial deformation along the [001] direction, C_{12} is the pure shear stress at (110) crystal plane along the [110] direction, and C_{44} is a pure shear deformation on the (100) crystal plane[4]. The values of these three elastic constants for all compounds are summarized in Table 2. For $Gd_2Zr_2O_7$, our calculated values of C_{11}, C_{12} and C_{44} are 325.6, 126.3 and 94.0 GPa, respectively, which are found to be close to the results of $C_{11} = 314.2$ GPa, $C_{12} = 126.2$ GPa and $C_{44} = 96.2$ GPa for $Sm_2Zr_2O_7$. It should be pointed out that in this study the Gd 4*f* and Sm 4*f* electrons are treated as core electrons. In order to investigate if these *f* electrons will influence the mechanical properties of $Gd_2Zr_2O_7$ and $Sm_2Zr_2O_7$, we further consider the Gd 4*f* and Sm 4*f* electrons as valence electrons and carry out LDA + U calculations, in which the effective U values are taken to be 6 eV for Gd 4*f* and 8 eV for Sm 4*f* electrons[4]. For $Gd_2Zr_2O_7$, the LDA + U results of $C_{11} = 316.9$ GPa, $C_{12} = 123.0$ GPa and $C_{44} = 94.7$ GPa are very similar to the LDA calculations. In the case of $Sm_2Zr_2O_7$, the calculated $C_{11} = 276.9$ GPa, $C_{12} = 114.2$ GPa, and $C_{44} = 112.6$ GPa are deviated from the LDA results. Further investigation shows that the $Sm_2Zr_2O_7$ is elastically anisotropic, which is not consistent with the elastic isotropy of $Sm_2Zr_2O_7$. Hence, the Gd 4*f* and Sm 4*f* electrons are frozen in our calculations and all the calculations are carried out by the LDA method. These results indicate that $Gd_2Zr_2O_7$ and $Sm_2Zr_2O_7$ may exhibit very similar mechanical

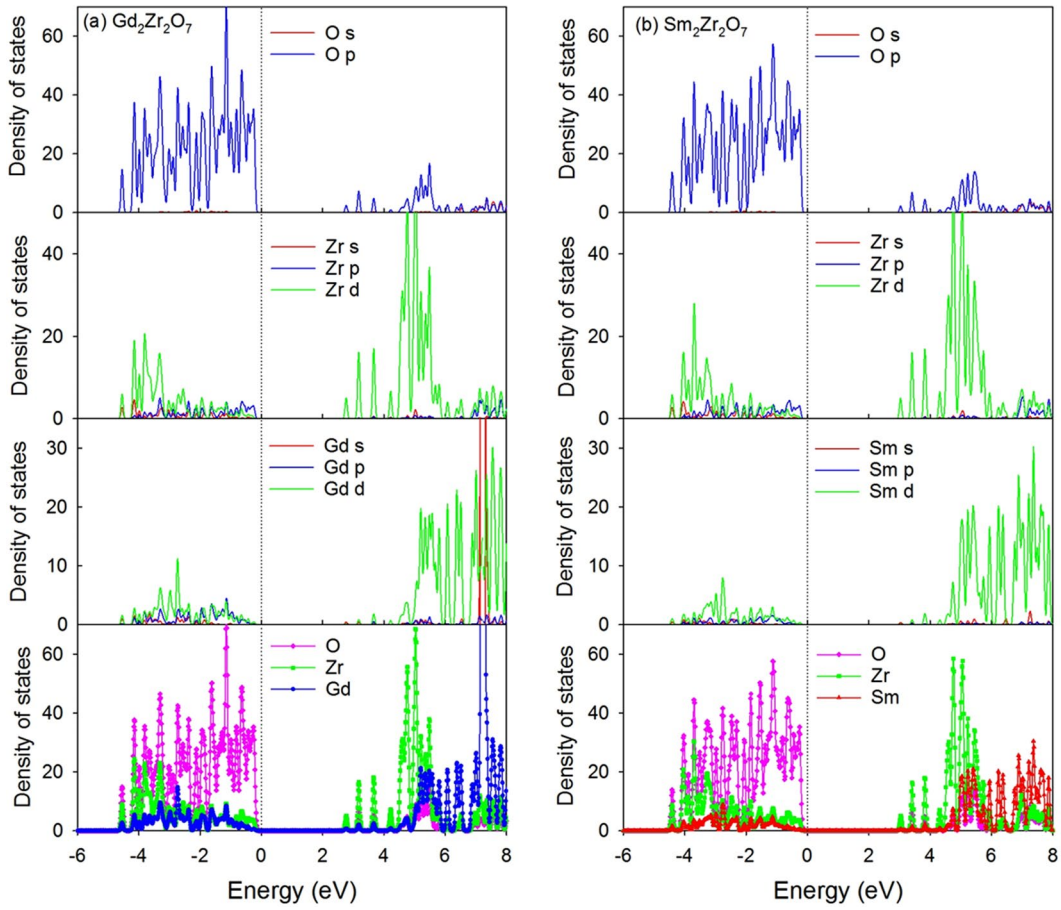

Figure 7. Projected density of state distribution for $Gd_2Zr_2O_7$ and $Sm_2Zr_2O_7$. The Fermi level is located at 0 eV.

properties, agreeing well with the experiment carried out by Shimamura *et al.*[20]. The elastic constants reported by Lan *et al.* employing GGA method are generally smaller than our LDA results, while they also found that the results of $Gd_2Zr_2O_7$ and $Sm_2Zr_2O_7$ are very similar to each other[36]. We find that the mechanical stability criteria, i.e., $(C_{11}\text{-}C_{12}) > 0$, $C_{44} > 0$, and $(C_{11} + 2C_{12}) > 0$[1], are satisfied for all compounds, indicating that Sm-substituted $Gd_2Zr_2O_7$ compounds are mechanically stable.

The calculated elastic constants for both $Sm_yGd_{2-y}Zr_2O_7$ and $Gd_2Sm_yZr_{2-y}O_7$ ($0 \le y \le 2$) as a function of Sm content are plotted in Fig. 3. It is noted that Sm substitution for Gd-site results in very small changes in the elastic constants and the mixed $Gd_2Zr_2O_7$-$Sm_2Zr_2O_7$ phases have similar values with the pure states. As the Sm substitutes for Zr-site, the values of C_{11} are strikingly decreased with the increasing Sm content, implying that the compositions with high content of Sm are more likely to undergo the uniaxial deformation along the [001] direction. On the other hand, the C_{12} and C_{44} slightly increase and decrease with the Sm incorporation, respectively. Generally, the changes in the elastic constants of $Gd_2Sm_yZr_{2-y}O_7$ are more significant than those of $Sm_yGd_{2-y}Zr_2O_7$, meaning that the effects of Sm incorporation into Gd-site on the mechanical properties of $Gd_2Zr_2O_7$ are nearly negligible whereas Sm incorporation into Zr-site has remarkable influence. This may be mainly due to the fact that Gd^{3+} and Sm^{3+} have similar mass (Gd^{3+}: 157.25 amu; Sm^{3+}: 150.3 amu) and cation size (Gd^{3+}: 1.053 Å; Sm^{3+}: 1.079 Å) and Sm substitution for Gd-site affects the structural properties of $Gd_2Zr_2O_7$ slightly, while the mass and radius for Gd^{3+} are largely different from the mass of 91.22 amu and the radius of 0.72 Å for Zr^{4+}[19,27] and an order-disorder phase transition has occurred in $Gd_2Sm_yZr_{2-y}O_7$.

Based on the three elastic constants, the bulk modulus (B), Young's modulus (E) and shear modulus (G) can be deduced under Voigt-Reuss-Hill (VRH) approximation[37], i.e., $B = (C_{11} + 2C_{12})/3$, $E = 9BG/(3B + G)$, $G = ((C_{11}\text{-}C_{12} + 3C_{44})/5 + 5(C_{11}\text{-}C_{12})C_{44}/(4C_{44} + 3(C_{11}\text{-}C_{12})))/2$[1,38–40]. The values of bulk modulus, Young's modulus and shear modulus are shown in Table 2, together with available experimental and theoretical results in the literature[20,36]. As compared with the experimental measurement, our calculated elastic moduli for $Gd_2Zr_2O_7$ and $Sm_2Zr_2O_7$ are overestimated slightly. This may be resulted from the employed LDA method, which generally underestimates the lattice constant whereas overestimates the mechanical modulus[41]. Besides, the defects and impurities in the sample experimentally may also lead to the underestimated values of the B and G[41]. Variation of the elastic moduli for $Sm_yGd_{2-y}Zr_2O_7$ and $Gd_2Sm_yZr_{2-y}O_7$ with the Sm content is illustrated in Fig. 4. As expected, the elastic moduli for $Sm_yGd_{2-y}Zr_2O_7$ vary slightly with the Sm content since the elastic constants for all compositions are very similar to each other. Different from the case of $Sm_yGd_{2-y}Zr_2O_7$, the bulk modulus, Young's modulus and shear modulus for $Gd_2Sm_yZr_{2-y}O_7$ all decrease sharply with the increasing Sm content, especially the Young's modulus.

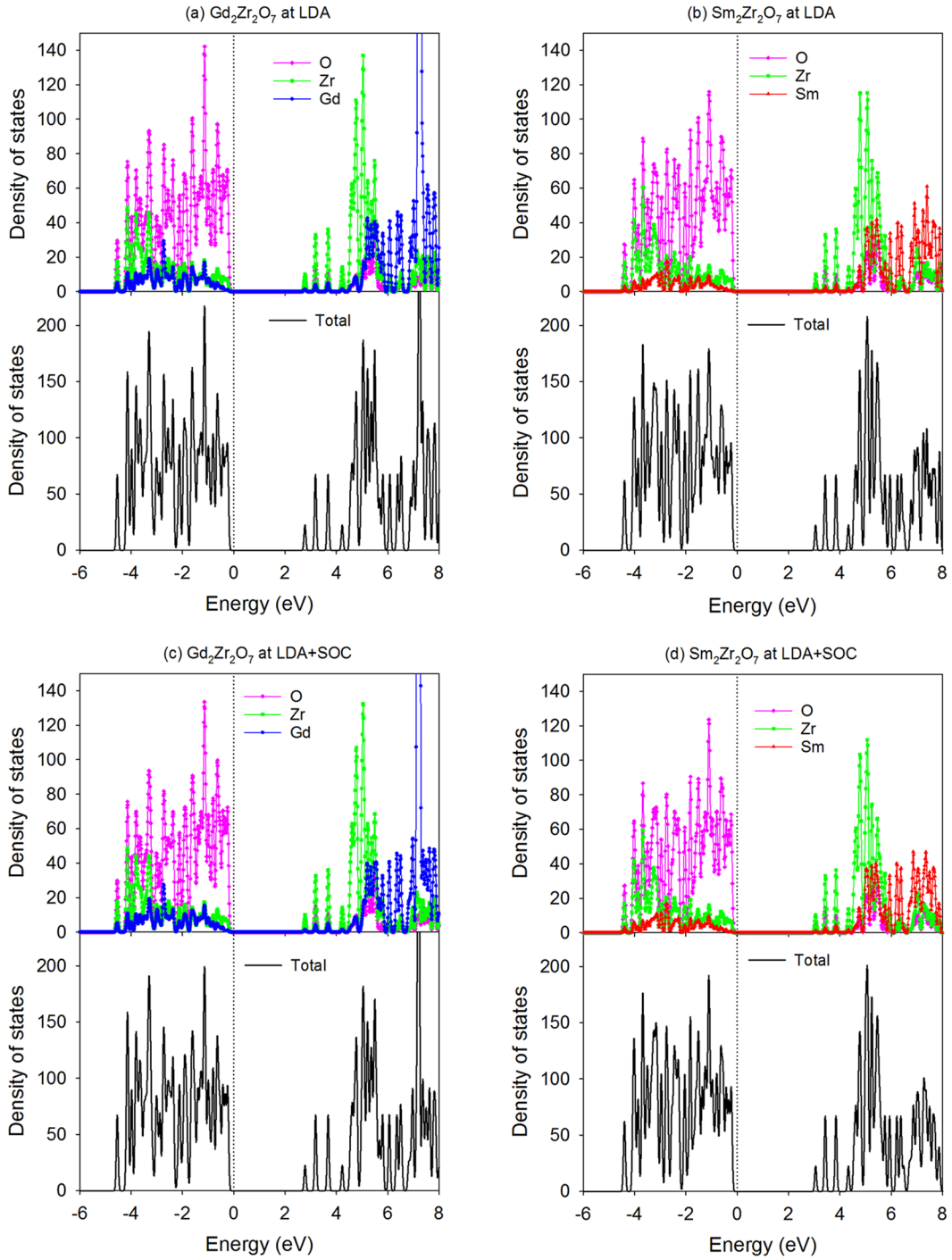

Figure 8. Projected and total density of state distribution for $Gd_2Zr_2O_7$ and $Sm_2Zr_2O_7$ obtained by the LDA and LDA + SOC methods. The Fermi level is located at 0 eV.

Consequently, the $Gd_2Sm_2O_7$ has the minimum Young's modulus of 87 GPa, minimum shear modulus of 31 GPa and minimum bulk modulus of 151 GPa. These results indicate that the $Gd_2Sm_2O_7$ has good compliance[2] due to the lowest bulk modulus and the lowest Young's modulus, which will produce relatively smaller residual stresses in the coating system under the severe conditions and result in better thermo-mechanical stability[23].

Elastic anisotropy, ductility and Debye temperature of $Sm_yGd_{2-y}Zr_2O_7$ and $Gd_2Sm_yZr_{2-y}O_7$ ($0 \leq y \leq 2$). The elastic anisotropy, which is correlated with the possibility of the appearance of microcracks, is an important mechanical property of materials[42,43]. For a crystal, the elastic anisotropy of materials can be evaluated by the A^U (universal elastic anisotropy index), which can be calculated by $A^U = 5\,G^V/G^R + B^V/B^R - 6$[44], with V and R representing the Voigt and Reuss approximation, respectively[38,40]. The A^U value of zero refers to isotropic

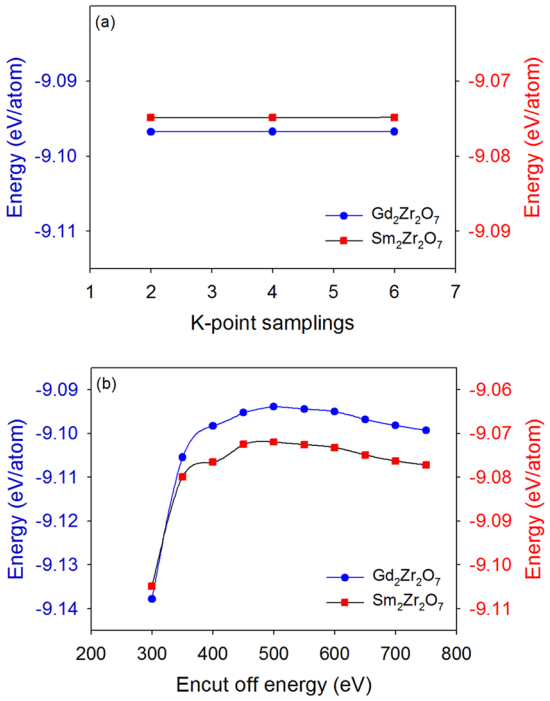

Figure 9. Variation of the total energy of $Gd_2Zr_2O_7$ and $Sm_2Zr_2O_7$ with (**a**) k-point sampling (the cutoff energy is fixed at 650 eV) and (**b**) cutoff energy (the k-point sampling is fixed at $2 \times 2 \times 2$).

mechanical properties, otherwise defines the anisotropy[44]. The calculated results are shown in Table 3. Obviously, the values of A^U are very close to zero in the case of $Sm_yGd_{2-y}Zr_2O_7$ ($0 \leq y \leq 2$), which indicates that all compounds are of elastic isotropy. However, the crystals show strong anisotropy in the $Gd_2Sm_yZr_{2-y}O_7$ ($0.5 \leq y \leq 2$) system, as the A^U values have large deviation from zero and they increase with the increasing Sm content. The sharp increase from 0.920 for $Gd_2Sm_{1.5}Zr_{0.5}O_7$ to 4.738 for $Gd_2Sm_2O_7$ may be caused by the pyrochlore-to-defect fluorite structural transition.

Another important mechanical property of materials is the ductility, which is often evaluated by the Pugh's indicator (G/B ratio)[45]. The Pugh's indicator of 0.5 is a boundary of brittleness or ductility, i.e., if $G/B > 0.5$, the material tends to be brittle; otherwise, the material is ductile[46]. The calculated Pugh's indicators are presented in Table 3. For the compounds of $Sm_yGd_{2-y}Zr_2O_7$, the values are close to 0.5, and are located within the range of 0.499 to 0.505. As for $Gd_2Sm_yZr_{2-y}O_7$ ($y = 0.5, 1, 1.5, 2$), the G/B values of 0.205–0.428 are much smaller. Obviously, the $Gd_2Sm_yZr_{2-y}O_7$ compositions have better ductility than the $Sm_yGd_{2-y}Zr_2O_7$ compounds. The Poisson's ratio (σ) can also be used to evaluate the relative ductility of materials. Generally, the σ values are close to 0.1 and 0.33 for brittle covalent material and ductile metallic material, respectively[46,47]. The σ values are 0.286 and 0.284 for $Gd_2Zr_2O_7$ and $Sm_2Zr_2O_7$, respectively, which are comparable with the experimental data of 0.274–0.276 for $Gd_2Zr_2O_7$ and 0.277–0.278 for $Sm_2Zr_2O_7$[20,48]. As shown in Table 3, the Poisson's ratio are ~0.285 for $Sm_yGd_{2-y}Zr_2O_7$ and vary from 0.313 to 0.404 for $Gd_2Sm_yZr_{2-y}O_7$, meaning that the latter compositions are more ductile, which is consistent with the results obtained from the Pugh's indicator.

In this study, the Debye temperature that is related to the hardness and thermal expansion coefficient of materials[20,49] is also estimated for Sm-contained $Gd_2Zr_2O_7$ by $\Theta = \frac{h}{k_B}\left[\frac{3n}{4\pi}\left(\frac{N_A\rho}{M}\right)\right]^{\frac{1}{3}} v_m$. Here, h is the Planck's constant, k_B is the Boltzmann's constant, n is the number of atoms in molecular, N_A is the Avogadro's constant, ρ is the density, M is the molecular mass and v_m is the sound wave velocity. The v_m can be deduced by $v_m = \left(\frac{3(v_t v_l)^3}{2v_t^3 + v_l^3}\right)^{\frac{1}{3}}$, where $v_l = \left(\frac{B + 4G/3}{\rho}\right)^{\frac{1}{2}}$ is the longitudinal sound velocity and $v_t = \left(\frac{G}{\rho}\right)^{\frac{1}{2}}$ is the transverse sound velocity[41]. As one can see from Table 3, Sm substitution for Gd-site has slight effects on the Debye temperature of $Gd_2Zr_2O_7$ and all the compositions have very similar results. However, as Sm substitutes for the Zr-site, the Debye temperature decreases considerably with the increasing Sm content. The $Gd_2Sm_2O_7$ has the lowest Debye temperature of 341.7 K, which is about 44.3% lower than that of $Gd_2Zr_2O_7$. These results suggest that Sm incorporation into Zr-site causes weaker interaction of chemical bonds and the $Gd_2Sm_yZr_{2-y}O_7$ with high content of Sm will have much larger thermal expansion coefficient than $Gd_2Zr_2O_7$.

Electronic structure of $Sm_yGd_{2-y}Zr_2O_7$ and $Gd_2Sm_yZr_{2-y}O_7$ ($0 \leq y \leq 2$). In order to investigate how Sm incorporation influences the electronic structure of $Gd_2Zr_2O_7$, the atomic projected density of state (DOS) distribution of $Sm_yGd_{2-y}Zr_2O_7$ and $Gd_2Sm_yZr_{2-y}O_7$ are analyzed and plotted in Fig. 5 and Fig. 6, respectively.

In Fig. 7a and b, the orbital projected DOS for $Gd_2Zr_2O_7$ and $Sm_2Zr_2O_7$ are also presented. For $Gd_2Zr_2O_7$, the valence band maximum (VBM) are mainly contributed by O 2*p* states hybridized with Zr 4*d*, Gd 5*d* and Gd 5*p* orbitals, and the conduction band minimum (CBM) are mainly contributed by Zr 4*d* states and O 2*p* states. The obtained band gap of 2.55 eV is comparable with the value of 2.71 eV reported by Wang *et al.*[50]. For $Sm_2Zr_2O_7$, the DOS distribution is similar to that of $Gd_2Zr_2O_7$, i.e., the VBM are mainly contributed by O 2*p* states hybridized with Zr 4*d*, Sm 5*d* and Sm 5*p* states, and the CBM are mainly dominated by Zr 4*d* states and O 2*p* states. Considering that Sm and Gd are heavy atoms and the spin-orbit coupling (SOC) may affect the band gap and electronic structure of the investigated systems, we further calculate the density of state distribution of $Gd_2Zr_2O_7$ and $Sm_2Zr_2O_7$ employing the LDA + SOC method. A comparison of LDA and LDA + SOC results for both compounds is illustrated in Fig. 8. For $Gd_2Zr_2O_7$, the band gap value of 2.64 eV by LDA + SOC is close to the value of 2.55 eV by LDA method. In the case of $Sm_2Zr_2O_7$, the band gap values are 2.9 eV and 2.83 eV for LDA + SOC and LDA calculations, respectively. As shown in Fig. 8, the atomic projected and total DOS obtained by LDA with and without spin-orbit coupling exhibit very similar characters for both compounds. These results suggest that the spin-orbit coupling has slight effects on our results and such effects are thus not considered for the mixed states. When Sm substitutes for Gd-site, the Sm 5*d* orbitals also contribute to the VBM and interacts with the oxygen. Meanwhile, the insulating character of $Gd_2Zr_2O_7$ is kept and the band gap is broadened with the increasing Sm content, i.e., 2.62, 2.68, 2.76 and 2.83 eV for $Sm_{0.5}Gd_{1.5}Zr_2O_7$, $SmGdZr_2O_7$, $Sm_{1.5}Gd_{0.5}Zr_2O_7$ and $Sm_2Zr_2O_7$, respectively. In addition, the hybridization of O 2*p* and Zr 4*d* is slightly affected by the incorporation of Sm. As for $Gd_2Sm_yZr_{2-y}O_7$, the hybridization of O 2*p* states with Zr 4*d*, Gd 5*d* and Sm 5*d* orbitals also dominates the VBM. It is interesting to find that Sm incorporation causes electrons distributing on the fermi levels and the number of electrons increases with the increasing Sm content. This results in an insulating-to-metallic transition and the $Gd_2Sm_yZr_{2-y}O_7$ has much stronger electronic conductivity than the pure state. In the meantime, the $Gd_2Zr_2O_7$ and $Sm_yGd_{2-y}Zr_2O_7$ do not have any magnetism, whereas the $Gd_2Sm_yZr_{2-y}O_7$ compositions exhibit strong ferromagnetic states due to the different charge states of Sm and Zr.

Obviously, Sm incorporation into Gd-site and Zr-site of $Gd_2Zr_2O_7$ causes very different electronic structures, i.e., the $Sm_yGd_{2-y}Zr_2O_7$ and $Gd_2Sm_yZr_{2-y}O_7$ are mainly of insulating and metallic characters, respectively. These results indicate that the thermal conductivity of $Sm_yGd_{2-y}Zr_2O_7$ are mainly contributed by phonons, while both phonons and electrons contribute to the thermal conductivity of $Gd_2Sm_yZr_{2-y}O_7$.

Summary

In this work, a systematic study based on the DFT method is carried out to investigate the effects of Sm substitution for Gd-site and Zr-site in $Gd_2Zr_2O_7$ on its structural stability, mechanical properties, Debye temperature and electronic structures. It is shown that the $Sm_yGd_{2-y}Zr_2O_7$ compositions keep the pyrochlore structure and their lattice parameters follow well the Vegard's law, indicative of the formation of $Gd_2Zr_2O_7$-$Sm_2Zr_2O_7$ solid solution. On the other hand, Sm substitution for Zr-site influences the structure significantly and a pyrochlore-to-defect fluorite structural transition occurs. The $Sm_yGd_{2-y}Zr_2O_7$ compositions are of elastic isotropy and their elastic moduli, ductility, Debye temperature and band gap vary slightly with the Sm content. However, the $Gd_2Sm_yZr_{2-y}O_7$ compounds show strong elastic anisotropy and their bulk, Young's and shear moduli all decrease sharply with the increasing Sm content. Consequently, the $Gd_2Sm_2O_7$ has the minimum Young's modulus of 87 GPa, minimum shear modulus of 31 GPa and minimum bulk modulus of 151 GPa. Meanwhile, both the Pugh's indicator and Poisson's ratio suggested that the $Gd_2Sm_yZr_{2-y}O_7$ have better ductility than the $Sm_yGd_{2-y}Zr_2O_7$. As the Sm substitutes for Zr-site, the Debye temperature decreases considerably with the increasing Sm content and the Debye temperature of 341.7 K for $Gd_2Sm_2O_7$ is about 44.3% lower than that of $Gd_2Zr_2O_7$. In addition, the insulating character of $Gd_2Zr_2O_7$ is kept in the system of $Sm_yGd_{2-y}Zr_2O_7$, while the $Gd_2Sm_yZr_{2-y}O_7$ compositions exhibit metallic characters. Our calculations demonstrate that substituting Sm for Zr-site is an effective approach to tailor the mechanical and thermal properties of $Gd_2Zr_2O_7$.

Methods

In this work, first-principles total energy calculations within the DFT framework are carried out. All calculations are performed with the Vienna Ab-initio Simulation Package (VASP)[51,52]. The interaction between electrons and ions is described by the projector augmented wave method[52,53]. All computations are based on a supercell containing 88 atoms. The convergence criteria for total energies and forces are 10^{-6} eV and 10^{-6} eV/Å, respectively. The structural relaxation is carried out at variable volume. In order to determine the values of cutoff energy and k-point sampling, a series of test calculation has been carried out. Figure 9 shows the variation of total energy of $Gd_2Zr_2O_7$ and $Sm_2Zr_2O_7$ with cutoff energy and k-point sampling, which leads to our calculation being performed with a $2 \times 2 \times 2$ Monkhorst-Pack k-mesh for Brillouin-zone integrations and a cutoff energy of 600 eV for plane wave. For $Sm_yGd_{2-y}Zr_2O_7$ and $Gd_2Sm_yZr_{2-y}O_7$ (y = 0.5, 1, 1.5), the structure models are constructed by the special quasirandom structure approach[54–56].

References

1. Zhao, F. A., Xiao, H. Y., Jiang, M., Liu, Z. J. & Zu, X. T. A DFT + U study of Pu immobilization in $Gd_2Zr_2O_7$. *J. Nucl. Mater.* **467**, 937–948 (2015).
2. Schelling, P. K., Phillpot, S. R. & Grimes, R. W. Optimum pyrochlore compositions for low thermal conductivity. *Philos. Mag. Lett.* **84**, 127–137 (2004).
3. Liu, Z. G., Ouyang, J. H., Zhou, Y. & Xia, X. L. Effect of Sm substitution for Gd on the electrical conductivity of fluorite-type $Gd_2Zr_2O_7$. *J. Power Sources* **185**, 876–880 (2008).
4. Feng, J. *et al.* Electronic structure, mechanical properties and thermal conductivity of $Ln_2Zr_2O_7$ (Ln = La, Pr, Nd, Sm, Eu and Gd) pyrochlore. *Acta. Mater.* **59**, 1742–1760 (2011).
5. Sohn, J. M., Kim, M. R. & Woo, S. I. The catalytic activity and surface characterization of $Ln_2B_2O_7$ (Ln = Sm, Eu, Gd and Tb; B = Ti or Zr) with pyrochlore structure as novel CH_4 combustion catalyst. *Catal. Today.* **83**, 289–297 (2003).

6. Shionzaki, K. *et al*. Oxygen-Ion Conduction in the $Sm_2Zr_2O_2$ Pyrochlore. *J. Am. Ceram. Soc.* **62**, 538–539 (1979).
7. Hatnean, M. C. *et al*. Structural and magnetic investigations of single-crystalline neodymium zirconate pyrochlore $Nd_2Zr_2O_7$. *Phys. Rev. B* **91**, 174416 (2015).
8. Singh, V. K. *et al*. Optical Studies of Erbium and Ytterbium Doped $Gd_2Zr_2O_7$ Phosphor for Display and Optical Communication Applications. *J. Disp. Technol.* **12**, 5 (2016).
9. Clarke, D. R. Materials selection guidelines for low thermal conductivity thermal barrier coatings. *Surf. Coat. Technol.* **163–164**, 67–74 (2003).
10. Clarke, D. R. & Phillpot, S. R. Thermal barrier coating materials. *Mater. Today* **8**, 22–29 (2005).
11. Xiao, H. Y., Weber, W. J., Zhang, Y. & Zu, X. T. Ab initio molecular dynamics simulations of ion–solid interactions in zirconate pyrochlores. *Acta. Mater.* **87**, 273–282 (2015).
12. Fergus, J. W. Electrolytes for solid oxide fuel cells. *J. Power Sources* **162**, 30–40 (2006).
13. Ewing, R. C., Weber, W. J. & Lian, J. Nuclear waste disposal—pyrochlore ($A_2B_2O_7$): Nuclear waste form for the immobilization of plutonium and "minor" actinides. *J. Appl. Phys.* **95**, 5949–5971 (2004).
14. Moon, P. K. & Tuller, H. L. Evaluation of the $Gd_2(ZrxTi1\text{-}x)_2O_7$ pyrochlore system as an oxygen gas sensor. *Sensor. actuat. B: Chem.* **1**, 199–202 (1990).
15. Cao, X. Q., Vassen, R. & Stoever, D. Ceramic materials for thermal barrier coatings. *J. Eur. Ceram. Soc.* **24**, 1–10 (2004).
16. Kutty, K. V. G., Rajagopalan, S. & Mathews, C. K. Thermal expansion behaviour of some rare earth oxide pyrochlores. *Mater. Res. Bull.* **29**, 759–766 (1994).
17. Feng, J., Xiao, B., Zhou, R. & Pan, W. Thermal conductivity of rare earth zirconate pyrochlore from first principles. *Scripta. Mater.* **68**, 727–730 (2013).
18. Wan, C. L. *et al*. Effect of point defects on the thermal transport properties of$(La_xGd_{1-x})_2Zr_2O_7$: Experiment and theoretical model. *Phys. Rev. B* **74**, 144109 (2006).
19. Liu, Z.-G., Ouyang, J.-H. & Zhou, Y. Structural evolution and thermophysical properties of $(Sm_xGd_{1-x})_2Zr_2O_7$ ($0 \leq x \leq 1.0$) ceramics. *J. Alloy Compd.* **472**, 319–324 (2009).
20. Shimamura, K., Arima, T., Idemitsu, K. & Inagaki, Y. Thermophysical Properties of Rare-Earth-Stabilized Zirconia and Zirconate Pyrochlores as Surrogates for Actinide-Doped Zirconia. *Int. J. Thermophys.* **28**, 1074–1084 (2007).
21. Wang, J. D., Pan, W., Xu, Q., Mori, K. & Torigoe, T. Thermal Conductivity of the New Candidate Materials for Thermal Barrier Coatings. *Key Eng. Mater.* **280–283**, 1503–1506 (2005).
22. Wang, C., Guo, L., Zhang, Y., Zhao, X. & Ye, F. Enhanced thermal expansion and fracture toughness of Sc_2O_3-doped $Gd_2Zr_2O_7$ ceramics. *Ceram. Int.* **41**, 10730–10735 (2015).
23. Pan, W., Wan, C. L., Xu, Q., Wang, J. D. & Qu, Z. X. Thermal diffusivity of samarium–gadolinium zirconate solid solutions. *Thermochim. Acta* **455**, 16–20 (2007).
24. Wang, X., Guo, L., Zhang, H., Gong, S. & Guo, H. Structural evolution and thermal conductivities of $(Gd_{1-x}Yb_x)2Zr_2O_7$ ($x = 0$, 0.02, 0.04, 0.06, 0.08, 0.1) ceramics for thermal barrier coatings. *Ceram. Int.* **41**, 12621–12625 (2015).
25. Liu, Z.-G., Ouyang, J.-H. & Zhou, Y. Preparation and thermophysical properties of $(Nd_xGd_{1-x})_2Zr_2O_7$ ceramics. *J. Mater. Sci.* **43**, 3596–3603 (2008).
26. Guo, L., Guo, H., Peng, H. & Gong, S. Thermophysical properties of Yb_2O_3 doped $Gd_2Zr_2O_7$ and thermal cycling durability of $(Gd_{0.9}Yb_{0.1})_2Zr_2O_7$/YSZ thermal barrier coatings. *J. Eur. Ceram. Soc.* **34**, 1255–1263 (2014).
27. Schelling, P. K. Thermal conductivity of A-site doped pyrochlore oxides studied by molecular-dynamics simulation. *Comp. Mater. Sci.* **48**, 336–342 (2010).
28. Zhao, F. A., Xiao, H. Y., Liu, Z. J., Li, S. & Zu, X. T. A DFT study of mechanical properties, thermal conductivity and electronic structures of Th-doped $Gd_2Zr_2O_7$. *Acta. Mater.* **121**, 299–309 (2016).
29. Ceperley, D. M. & Alder, B. J. Ground State of the Electron Gas by a Stochastic Method. *Phys. Rev. Lett.* **45**, 566–569 (1980).
30. Perdew, J. P., Burke, K. & Ernzerhof, M. Generalized Gradient Approximation Made Simple. *Phys. Rev. Lett.* **77**, 3865–3868 (1996).
31. Lian, J. *et al*. Ion-irradiation-induced amorphization of $La_2Zr_2O_7$ pyrochlore. *Phys. Rev. B* **66**, 054108 (2002).
32. Wang, C. *et al*. Preparation and thermophysical properties of nano-sized $Ln_2Zr_2O_7$ (Ln = La, Nd, Sm, and Gd) ceramics with pyrochlore structure. *J. Mater. Sci.* **47**, 4392–4399 (2012).
33. Wang, X. J., Xiao, H. Y., Zu, X. T. & Weber, W. J. A DFT plus U study of cerium solubility in $La_2Zr_2O_7$. *J. Nucl. Mater.* **424**, 69–74 (2012).
34. Lian, J. *et al*. Radiation-induced amorphization of rare-earth titanate pyrochlores. *Phys. Rev. B* **68**, 134107 (2003).
35. Xiao, H. Y., Gao, F. & Weber, W. J. Ab initio investigation of phase stability of $Y_2Ti_2O_7$ and $Y_2Zr_2O_7$ under high pressure. *Phys. Rev. B* **80**, 212102 (2009).
36. Lan, G., Ouyang, B. & Song, J. The role of low-lying optical phonons in lattice thermal conductance of rare-earth pyrochlores: A first-principle study. *Acta. Mater.* **91**, 304–317 (2015).
37. Chung, D. H. The Voigt-Reuss-Hill (VRH) Approximation and the Elastic Moduli of Polycrystalline ZnO, TiO_2 (Rutile), and α-Al_2O_3. *J. Appl. Phys.* **39**, 2777–2782 (1968).
38. Reuss, A. & Angew, Z. Berechnung der Fliehgrenze von Mischkristallen auf Grund der Plastizittitsbedingung fiir Einkristalle. *Math. Phys.* **9**, 49–58 (1929).
39. Hill, R. The Elastic Behaviour of a Crystalline Aggregate. *Proc. Phy. Soc. A* **65**, 349–354 (1952).
40. Voigt, W. Über die Beziehung zwischen den beiden Elasticitätsconstanten isotroper Körper. *Ann. Phys.* **274**, 573–587 (1889).
41. Yang, J. *et al*. Physical properties of $La_2B_2O_7$ (B = Zr, Sn, Hf and Ge) pyrochlore: First-principles calculations. *J. Alloys Compd.* **663**, 834–841 (2016).
42. Tvergaard, V. & Hutchinson, J. W. Microcracking in Ceramics Induced by Thermal Expansion or Elastic Anisotropy. *J. Am. Ceram. Soc.* **71**, 157–166 (1988).
43. Ravindran, P. *et al*. Density functional theory for calculation of elastic properties of orthorhombic crystals: Application to $TiSi_2$. *J. Appl. Phys.* **84**, 4891–4904 (1998).
44. Ranganathan, S. I. & Ostoja-Starzewski, M. Universal elastic anisotropy index. *Phys. Rev. Lett.* **101**, 055504 (2008).
45. Pugh, S. F. Relations between the elastic moduli and the plastic properties of polycrystalline pure metals. *Philos. Mag.* **45**, 823–843 (1954).
46. Bannikov, V. V., Shein, I. R. & Ivanovskii, A. L. Elastic and electronic properties of hexagonal rhenium sub-nitrides Re_3N and Re_2N in comparison with hcp-Re and wurtzite-like rhenium mononitride ReN. *Phys. Status Solidi B* **248**, 1369–1374 (2011).
47. Bannikov, V. V., Shein, I. R. & Ivanovskii, A. L. Elastic and electronic properties of hexagonal rhenium sub-nitrides Re_3N and Re_2N in comparison with hcp-Re and wurtzite-like rhenium mononitride ReN. *Phys. Status Solidi (b)* **248**, 1369–1374 (2011).
48. Dijik, M. Pv., Vries, K. Jd. & Burggraaf, A. J. Oxygen ion and mixed conductivity in compounds with the fluorote and pyrochlore structure. *Solid State Ionics* **9–10**, 913–920 (1983).
49. Childress, J. R., Chien, C. L., Zhou, M. Y. & Sheng, P. Lattice softening in nanometer-size iron particles. *Phys. Rev. B* **44**, 11689–11696 (1991).
50. Wang, J., Zhang, F., Lian, J., Ewing, R. C. & Becker, U. Energetics and concentration of defects in $Gd_2Ti_2O_7$ and $Gd_2Zr_2O_7$ pyrochlore at high pressure. *Acta. Mater.* **59**, 1607–1618 (2011).
51. Kresse, G. & Hafner, J. Ab inito molecular-dynamics for liquid-metals. *Phys. Rev. B* **47**, 558–561 (1993).

52. Kresse, G. & Furthmuller, J. Efficient iterative schemes for ab initio total-energy calculations using a plane-wave basis set. *Phys. Rev. B* **54**, 11169–11186 (1996).
53. Kresse, G. & Furthmiiller, J. Efficiency of ab-initio total energy calculations for metals and semiconductors using a plane-wave basis set. *Comp. Mater. Sci.* **6**, 15–50 (1996).
54. Zunger, A., Wei, S., Ferreira, L. G. & Bernard, J. E. Special quasirandom structures. *Phys. Rev. Lett.* **65**, 353–356 (1990).
55. Jiang, C., Wolverton, C., Sofo, J., Chen, L.-Q. & Liu, Z.-K. First-principles study of binary bcc alloys using special quasirandom structures. *Phys. Rev. B* **69**, 214202 (2004).
56. Jiang, C., Stanek, C. R., Sickafus, K. E. & Uberuaga, B. P. First-principles prediction of disordering tendencies in pyrochlore oxides. *Phys. Rev. B* **79**, 104203 (2009).
57. Guo, L., Li, M., Zhang, Y. & Ye, F. Improved Toughness and Thermal Expansion of Non-stoichiometry $Gd_{2-x}Zr_{2+x}O_{7+x/2}$ Ceramics for Thermal Barrier Coating Application. *J. Mater. Sci. Technol.* **32**, 28–33 (2016).

Acknowledgements

H.Y. Xiao was supported by the NSAF Joint Foundation of China (Grant No. U1530129) and the scientific research starting funding of University of Electronic Science and Technology of China (Grant No. Y02002010401085). Z.J. Liu was supported by National Natural Science Foundation of China (Grant No. 11464025) and the New Century Excellent Talents in University under Grant no. NCET-11–0906. The theoretical calculations were performed using the supercomputer resources at TianHe-1 located at National Supercomputer Center in Tianjin.

Author Contributions

H.X. and X.Z. designed the calculations. S.Z. conducted the calculations and wrote the manuscript. F.Z., M.J., Z.L. and H.Zhang contributed the discussion and interpretation of the results. All authors discussed the results and reviewed the manuscript.

Additional Information

Competing Interests: The authors declare that they have no competing interests.

Publisher's note: Springer Nature remains neutral with regard to jurisdictional claims in published maps and institutional affiliations.